Synthesis of an extra-large molecular sieve using proton sponges as organic structure-directing agents

Raquel Martínez-Franco[a], Manuel Moliner[a,1], Yifeng Yun[b], Junliang Sun[b,c], Wei Wan[b], Xiaodong Zou[b,1], and Avelino Corma[a,1]

[a]Instituto de Tecnología Química, Universidad Politécnica de Valencia, Consejo Superior de Investigaciones Científicas (UPV-CSIC), Valencia 46022, Spain; [b]Berzelii Centre EXSELENT on Porous Materials and Inorganic and Structural Chemistry, Department of Materials and Environmental Chemistry, Stockholm University, SE-106 91 Stockholm, Sweden; and [c]College of Chemistry and Molecular Engineering, Peking University, Beijing 100871, China

Edited by Mark E. Davis, California Institute of Technology, Pasadena, CA, and approved January 18, 2013 (received for review November 28, 2012)

The synthesis of crystalline microporous materials containing large pores is in high demand by industry, especially for the use of these materials as catalysts in chemical processes involving bulky molecules. An extra-large–pore silicoaluminophosphate with 16-ring openings, ITQ-51, has been synthesized by the use of bulky aromatic proton sponges as organic structure-directing agents. Proton sponges show exceptional properties for directing extra-large zeolites because of their unusually high basicity combined with their large size and rigidity. This extra-large–pore material is stable after calcination, being one of the very few examples of hydrothermally stable molecular sieves containing extra-large pores. The structure of ITQ-51 was solved from submicrometer-sized crystals using the rotation electron diffraction method. Finally, several hypothetical zeolites related to ITQ-51 have been proposed.

aluminophosphate | extra-large microporous materials | zeolite synthesis

There is great interest in metal-substituted zeotypes, not only because of the exceptional catalytic properties isolated metals can provide to microporous materials but also because the introduction of metals in framework positions may offer unique structural inorganic directing effects during nucleation–crystallization processes (1, 2). Indeed, the incorporation of heteroatoms, such as Be, Zn, and Ge, has allowed the synthesis of new molecular sieve structures with extra-large pores (corresponding to openings larger than 12-ring pores), containing small three- and four-ring units (3–6). These metals in tetrahedral coordination present the required angle and chemical bond flexibilities to stabilize those small building units and, consequently, the overall zeolitic framework (1, 2).

In the 1980s, researchers from Union Carbide reported the synthesis of aluminophosphates (AlPOs) (7). These zeotype materials are formed by tetrahedral Al and P atoms in strict alternation, connected by O atoms. Since this early achievement, many new AlPO-related materials with diverse architectures have been described (8–11). The discovery of the extra-large VPI-5 AlPO molecular sieve containing 18-ring channels was a remarkable breakthrough, being the first extra-large–pore crystalline material ever synthesized (12). Following VPI-5, other phosphate-related extra-large–pore molecular sieves have been described (13–17). Unfortunately, most of them lack stability because of features such as mixed-metal coordination (tetrahedral–octahedral), terminal OH groups, and the presence of nontetrahedral species (e.g., OH, H_2O, or F) (18).

Particularly intriguing is the small number of extra-large–pore microporous materials containing 16-ring channels. Although Curtis and Deem (19) predicted that these zeolitic structures are thermodynamically feasible, only three microporous materials with 16-rings have been reported. Of these three materials, two are oxyfluorinated gallium phosphates, ULM-5 (20) and ULM-16 (21), with gallium in diverse atomic coordination (tetrahedral and octahedral); the other is the germanium-rich ITQ-40 containing 16 × 16 × 15-rings and structural defects (22). More specifically, in the AlPO family, it is possible to find structures with 12-, 14-, and 18-rings, but AlPO structures with 16-rings have not been reported up to now, as far as we know.

Davis and colleagues (23–25) have used large and rigid organic structure-directing agents (OSDAs) to synthesize diverse extra-large–pore zeolites containing 14-ring channels. However, the design and preparation of new large and rigid OSDAs capable of directing extra-large–pore zeolites are not always easy; moreover, if the bulky OSDA is highly hydrophobic (very large size and high C/N ratio), organic–inorganic interactions in the nucleation–crystallization processes and solubility may not be adequate, resulting in amorphous materials during the synthesis (26).

Proton sponges—for example, commercially available 1,8-bis (dimethylamino)naphthalene (DMAN; Fig. 1)—are bulky aromatic diamines with amine groups in close proximity (27). These molecules present a highly unusual basicity because of the repulsion of the close electronic lone pairs ($pK_a \approx 12.1$) (28). They are used extensively in organic synthesis as very selective nonnucleophilic bases with very interesting catalytic properties when used in the homogeneous phase (29) or when prepared in the form of structured hybrid solid catalytic materials (30, 31). Taking into account their basic properties, the C/N ratio, and molecular structures, we thought proton sponges might be suitable OSDAs for the synthesis of extra-large microporous molecular sieves. Indeed, the high basicity showed by proton sponges allows their protonation, even at high pHs in the zeolitic synthesis media, favoring organic–inorganic interactions during zeolite nucleation and crystallization processes (32). Moreover, their large size and rigidity might be adequate for templating extra-large pores.

Most zeolites are synthesized as micro- or nano-sized crystals, which are too small or too complex to be studied by single-crystal diffraction or powder X-ray diffraction (PXRD). Electron crystallography is an important technique for studying such crystals (33–35). Crystals considered as powder by X-ray diffraction behave as single crystals by electron diffraction. Recently, we developed a method known as rotation electron diffraction (RED) for collecting 3D electron diffraction data by combining electron beam tilt and goniometer tilt on a transmission electron microscope (TEM) (36). This method is promising for both phase identification and structure determination of unknown micro- and nano-sized crystals.

Herein, we present the use of the bulky aromatic proton sponge DMAN as an OSDA to synthesize previously undescribed extra-large–pore silicoaluminophosphate (SAPO) with 16-ring openings, named ITQ-51. This zeolitic material shows extra-large

Author contributions: M.M., Y.Y., W.W., X.Z., and A.C. designed research; R.M.-F., M.M., and Y.Y. performed research; W.W. contributed new reagents/analytic tools; R.M.-F., M.M., Y.Y., J.S., and A.C. analyzed data; and M.M., Y.Y., X.Z., and A.C. wrote the paper.

The authors declare no conflict of interest.

This article is a PNAS Direct Submission.

[1]To whom correspondence may be addressed. E-mail: acorma@itq.upv.es, mmoliner@itq.upv.es, or xzou@mmk.su.se.

This article contains supporting information online at www.pnas.org/lookup/suppl/doi:10.1073/pnas.1220733110/-/DCSupplemental.

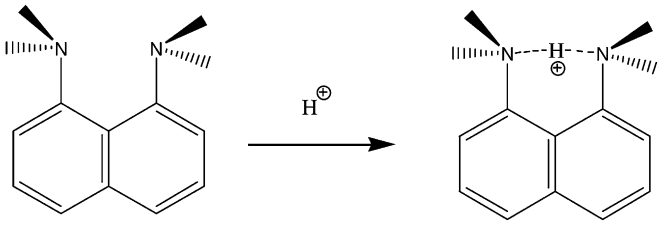

Fig. 1. Proton sponge DMAN.

pores with 16-ring openings and excellent hydrothermal stability. The structure of ITQ-51 has been elucidated by using the RED method.

Results and Discussion

Different molar gel compositions and temperatures have been studied using DMAN as an OSDA in the synthesis of AlPO and SAPO materials. As seen in Fig. 2, pure ITQ-51 material is achieved under specific synthesis conditions [Si/(Al + P) = 0.1, P/Al = 0.9, DMAN/(Al + P) = 0.3, H_2O/(Al + P) = 10, T = 150 °C]. At the two synthesis temperatures studied here, an unstable lamellar material is the preferred phase when lowering the water content [H_2O/(Al + P) = 5] and increasing the DMAN concentration [DMAN/(Al + P) = 0.5]. On the other hand, tridymite dense phase appears as an impurity when silicon is removed from the synthesis gel at the specific synthesis conditions of ITQ-51.

The PXRD patterns of the as-prepared ITQ-51 sample and the ITQ-51 sample air-calcined at 550 °C were collected (*SI Appendix*, Fig. S1). The high thermal stability of this unique material was confirmed further by PXRD at different temperatures under inert conditions from 100 °C to 700 °C (*SI Appendix*, Fig. S2). Scanning electron microscopy (SEM) images show plate-like aggregates with sizes ranging between 0.5 and 2 μm (*SI Appendix*, Fig. S3).

Elemental analyses were performed on the as-prepared ITQ-51, achieving a C/N molar ratio value of 6.8 [16.359% (wt/wt) C, 2.818% (wt/wt) N, 2.456% (wt/wt) H]. This value is very close to the expected C/N molar ratio for the DMAN molecule (C/N = 7), confirming that almost all template molecules remain intact within ITQ-51 crystals. In addition, solid-state ^{13}C magic-angle spinning (MAS) NMR of the as-prepared ITQ-51 also confirms that DMAN molecules are undamaged in the final solid (Fig. 3).

To study the textural properties of ITQ-51, N_2 and Ar adsorption measurements were performed on the calcined material. The *t*-plot method applied to the N_2 adsorption at 77 K reveals a micropore volume of 0.13 cm^3/g and a micropore area of 290 m^2/g. The total Brunauer-Emmet-Teller (BET) surface area is 367 m^2/g. The N_2 adsorption isotherm shows the characteristic shape of microporous materials (*SI Appendix*, Fig. S4). Interestingly, Ar adsorption at 87 K exhibits an experimental pore distribution calculated by applying the Horvath–Kawazoe formalism, centered at 7.4 Å (*SI Appendix*, Fig. S5). The adsorption data observed, both from Ar and N_2 adsorption measurements, would indicate that the framework structure of ITQ-51 may contain 1D extra-large (14- or 16-ring) pores.

^{27}Al, ^{29}Si, and ^{31}P MAS NMR spectra of the calcined ITQ-51 material were recorded to obtain information on the local atomic environments, which also may be very useful for structure elucidation. The ^{31}P MAS NMR spectrum shows at least four well-defined, distinct crystallographic positions for P atoms (*SI Appendix*, Fig. S6). The ^{27}Al MAS NMR spectrum shows a broad band between 20 and 45 ppm (*SI Appendix*, Fig. S7), clearly indicating that all aluminum species in the ITQ-51 molecular sieve are in tetrahedral coordination (no signal is observed close to 0 ppm, characteristic of Al in octahedral coordination). Additionally, the study of AlPOs by ^{27}Al multiple-quantum (MQ) MAS NMR allows truly high resolution of the distinct Al crystallographic sites present in the material (37). The 2D ^{27}Al MQ MAS spectra of ITQ-51 clearly show at least three different well-resolved Al sites (*SI Appendix*, Fig. S8). Finally, the ^{29}Si MAS NMR spectrum illustrates a single peak at −110 ppm, assigned to the presence of silicon atoms forming silicon-rich domains (*SI Appendix*, Fig. S9) (38).

The structure elucidation of ITQ-51 was carried out by the RED method (39). The 3D RED data were collected from several crystals with different orientations of both as-synthesized and calcined ITQ-51 samples using the RED data collection software (40). Two datasets from the as-synthesized ITQ-51, with >130° angle range and >1,300 electron diffraction (ED) frames each, cover different parts of the reciprocal lattice and thus are combined. Each dataset was processed using the RED data processing software (40), and the 3D reciprocal lattice of ITQ-51 was reconstructed from the RED data (*SI Appendix*, Fig. S10). The unit cell parameters of ITQ-51 could be determined from each of the datasets (*SI Appendix*, Table S1) and refined further by PXRD of the calcined ITQ-51 [a = 23.345(2) Å, b = 16.513(2) Å, c = 4.9814(5) Å, α = 90°, β = 90.620(5)°, γ = 90°]. The space group could be deduced from the systematic absences to be $P2_1/n$, as indicated from the 2D slices cut from the 3D RED data (*SI Appendix*, Fig. S11), which also was confirmed by PXRD data. The structure could be solved by direct methods from each of the two datasets (*SI Appendix*, Table S2). All eight symmetry-independent framework T atoms (Al, Si, or P) and 16 O atoms could be located. The framework structure could be refined against the 3D RED data, with R_1 = 0.37 for 2,310 independent reflections (81.8% completeness up to 0.90 Å) from the merged

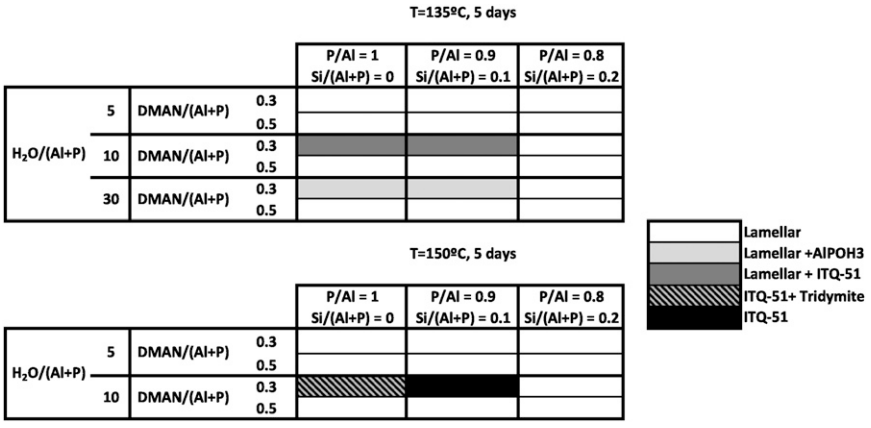

Fig. 2. Experimental conditions studied and phases achieved.

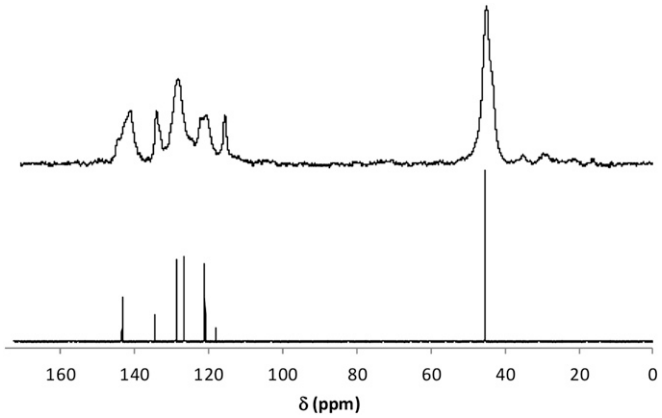

Fig. 3. Solid ^{13}C MAS NMR spectrum of as-prepared ITQ-51 molecular sieve (*Upper*) and liquid ^{13}C NMR spectrum of proton sponge DMAN (*Lower*).

RED dataset. It was possible to assign Al and P positions based on the differences in T–O distances. The underlying topology of the ITQ-51 framework is a unique four-connected zeolitic net with the highest topologic symmetry of *Pmnn*. The monoclinic framework of ITQ-51 was a result of the ordering of Al and P. The structure model was refined further by Rietveld refinement against the PXRD data of the calcined ITQ-51 sample. To get more stable refinement, the background from air scattering was fitted by a function (Background = I/θ) and then removed. Soft geometric restraints were applied on all T–O distances. The final refinement converged with the structure factor (R_F), weighted profile (R_{wp}), and statistically expected R-values of 1.2%, 8.2%, and 1.9%, respectively (*SI Appendix*, Table S2 and Fig. 4). After the Rietveld refinement, the T and O atoms were shifted on average by 0.11 Å and 0.13 Å, with a maximum shift of 0.16 Å and 0.23 Å, respectively, from the positions obtained from the RED data. This means that RED can give an excellent starting model, and the high R_1-value was mainly a result of the distortions of the intensities by multiple scattering.

ITQ-51 has a unique zeolite framework with 1D 16-ring channels along the c-axis with free diameters of 9.9 × 7.7 Å (Fig. 5). The framework is built from two different chains that share common TO_4 tetrahedra; the **lau** chain often found in zeolites (*SI Appendix*, Fig. S12*A*) and a unique helical four-ring chain (*SI Appendix*, Fig. S12*B*). The structure contains 4 symmetry-independent Al atoms, 4 symmetry-independent P atoms, and 16 symmetry-independent O atoms. Tetrahedral AlO_4 and PO_4 alternate in the structure and

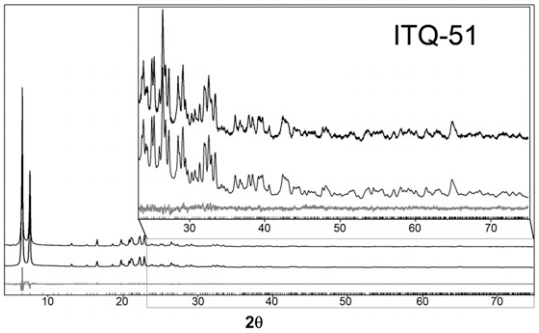

Fig. 4. Observed (*Upper*) and calculated (*Middle*) PXRD profiles, as well as the difference between observed and calculated profiles (*Lower*), for the Rietveld refinement of the calcined ITQ-51 (λ = 1.5406 Å). The higher-angle data have been scaled up (*Inset*) to show the good fit between the observed and calculated patterns.

are connected by corner sharing. Some Al and P positions are partially occupied by silicon. However, it was not possible to locate the Si positions and refine the occupancies because of the low Si content (on average, 8% (at/at) Si at each T-site from chemical analysis) and similar atomic scattering factors for Al, Si, and P. The framework density of ITQ-51 is 16.7 T atoms per 1,000 Å^3.

ITQ-51 is previously undescribed aluminophosphate zeotype containing 16-ring channels. In fact, zeolites with 16-ring pores are very rare; the only example is the germanosilicate ITQ-40 (22). ITQ-51 is one of the very few extra-large–pore zeolites with ≥16-ring channels that are stable in air after calcination. As far as we know, the other two zeolites are the galloaluminosilicate ECR-34 (ETR) (41) and the AlPO VPI-5 (VFI) (12), both with 18-ring channels. The pore size in ITQ-51 thus is very attractive for shape-selective applications.

The framework topology of ITQ-51 was predicted by Deem and coworkers (42) as a silica analog and may be found in the DEEM SLC GOOD database (43). A few other hypothetical zeolite frameworks containing 16-rings also are predicted in databases (42–44). The known zeolite in the database (45) that is mostly related to ITQ-51 is SAPO-31 (46), which contains 1D 12-ring channels and has a c-parameter (c = 5.003 Å) similar to that of ITQ-51 (Fig. 6*A*). If four of the six 4-rings forming the 12-ring channel in SAPO-31 are substituted with four helical 4-ring chains, the structure of ITQ-51 with oval 16-ring channels can be achieved easily (Fig. 6*B*). The **lau** composite building unit [$4^2 6^4$] may be found in both structures. Similarly, if all six of the 4-rings forming the 12-ring channel in AlPO-31 are substituted by six helical 4-ring chains, a hypothetical 18-ring zeolite (denoted as T18MR) is formed (Fig. 6*C*). The pore openings of AlPO-31, ITQ-51, and T18MR are 6.5 × 4.0 Å, 9.9 × 7.7 Å, and 11.2 × 10.5 Å, respectively. The hexagonal lattice remains in T18MR because of the substitution of all six 4-ring chains, the lattice of ITQ-51 becomes orthorhombic because only four of the 4-ring chains are substituted (*SI Appendix*, Table S3).

A similar approach may be used to predict new zeolite frameworks related to other zeolites. Davis et al. (12) illustrated that the topologies of the 12-ring AlPO-5 and 18-ring VPI-5 are highly related. The 1D 18-ring channel in VPI-5 is formed by six double narsarsukite chains (*SI Appendix*, Fig. S12*D*) that are connected, as shown in Fig. 6*F*. If each of the double narsarsukite chains in VPI-5 is replaced by a double crankshaft chain (*SI Appendix*, Fig. S12*C*), a hypothetical zeolite with 1D 12-ring channels is obtained (Fig. 6*D*, denoted as T12MR). The topology of T12MR previously was predicted as the **umk** net (47). Furthermore, similar to ITQ-51, if four of the six double narsarsukite chains forming the 18-ring channel in VPI-5 are replaced by double crankshaft chains, a hypothetical 1D 16-ring zeolite is obtained (Fig. 6*E*, denoted as T16MR). The pore openings of T12MR, T16MR, and VPI-5 are 7.5 × 7.5 Å, 11.8 × 11.8 Å, and 12.7 × 12.7 Å, respectively. The coordination sequences and vertex symbols for ITQ-51 and the three hypothetical zeolites are given in *SI Appendix*, Table S4.

The ITQ-51 zeotype not only shows an extra-large pore structure, it also fills the pore size gap of reported zeolitic materials (*SI Appendix*, Table S5), being described as an all tetrahedrally connected and hydrothermally stable molecular sieve with 16-ring pores. This combination opens an opportunity for synthesizing different metal-containing ITQ-51 zeotypes with well-defined acid and redox isolated sites, as described for other Me-AlPOs (11).

In conclusion, we have shown the use of proton sponges as potential OSDAs for the synthesis of zeolites. More specifically, they may be of interest for the synthesis of extra-large–pore molecular sieves. These possibilities are demonstrated clearly by the successful synthesis of the hydrothermally stable ITQ-51 containing 1D 16-ring pores. The ability to design proton sponges with different sizes, geometries, hydrophobicity, or basicity (27, 28) may open opportunities for the synthesis of new zeolitic materials.

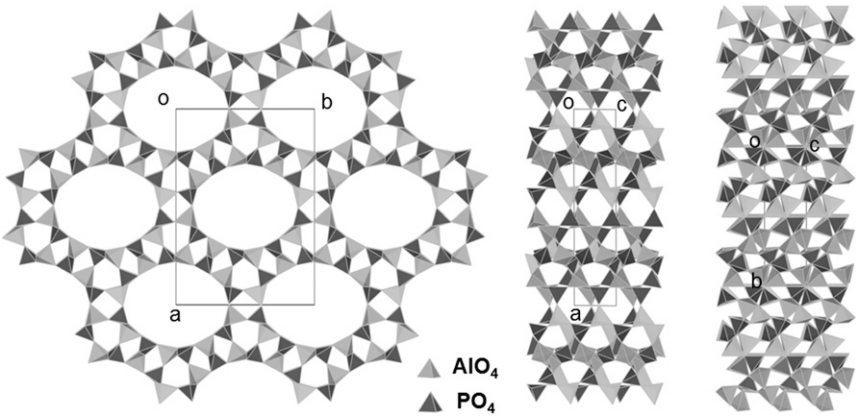

Fig. 5. Structure model for ITQ-51 molecular sieve viewed along (*Left*) the *c*-axis, (*Center*) the *b*-axis, and (*Right*) the *a*-axis.

Moreover, we have demonstrated a complete ab initio 3D structure solution of unknown zeolites from a single submicrometer-sized crystal using the RED method. The RED method is much more feasible than other TEM techniques, such as high-resolution TEM (HRTEM), and generally may be applied to any unknown nano-sized crystals, including beam-sensitive materials, because of

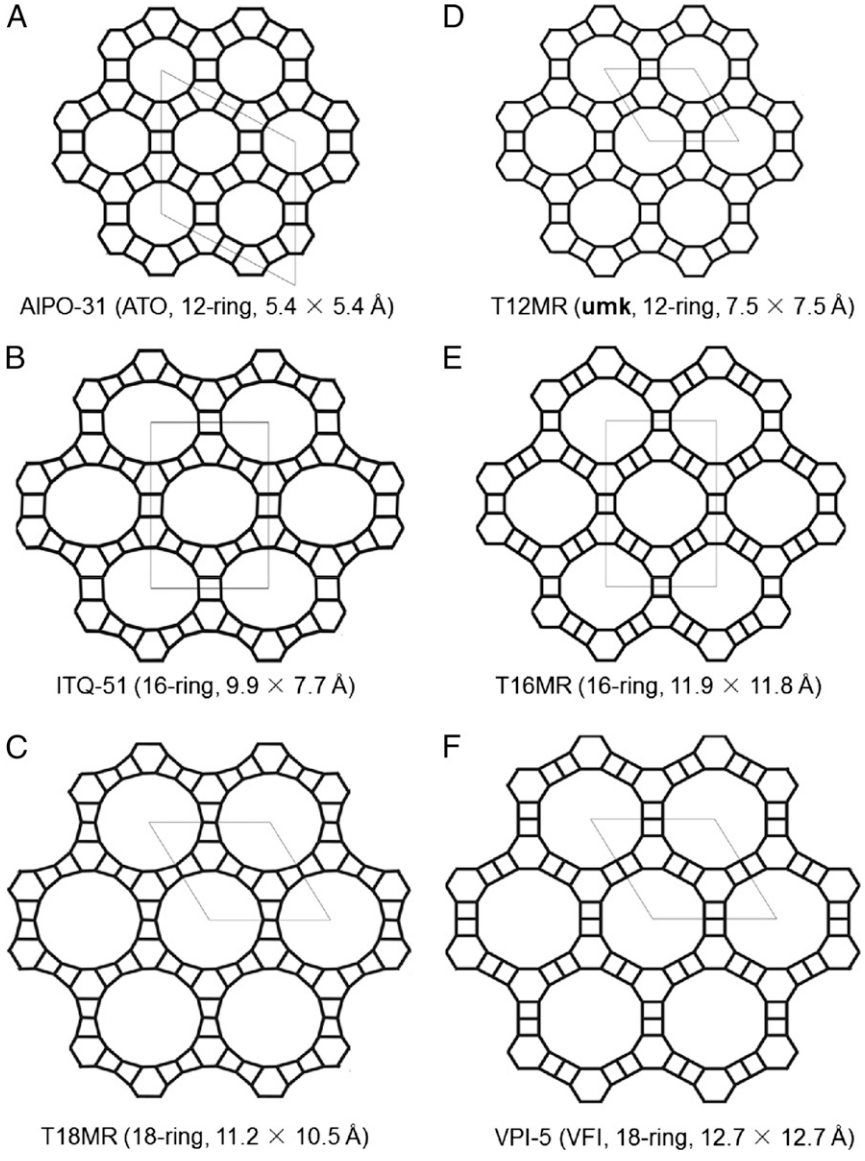

Fig. 6. Structures of AlPO-31 (*A*), ITQ-51 (*B*), hypothetical zeolite T18MR (*C*), hypothetical zeolite T12MR (*D*), hypothetical zeolite T16MR (*E*), and VPI-5 (*F*). Only T–T connections are shown for clarity.

the much lower electron dose required for electron diffraction compared with doses for HRTEM. Structure solution by the RED method is much faster and more feasible than that by PXRD because there is less ambiguity in determining unit cell and space group, and it is applicable to samples containing impurities. It even is comparable to that of single-crystal X-ray diffraction, but from crystals millions of times smaller.

Materials and Methods

Synthesis of ITQ-51 Zeolite. ITQ-51 was prepared using DMAN (99 wt%, Sigma-Aldrich) as OSDA. 257 mg of DMAN was mixed with 615 mg of distilled water and 218 mg of orthophosphoric acid (85 wt%; Sigma-Aldrich). This mixture was stirred for 2 h until complete dissolution of the OSDA. Then, 143 mg of alumina (75 wt%; Condea) and 60 mg of colloidal silica solution (Ludox AS-40, 40 wt%; Sigma-Aldrich) were introduced into the gel mixture and stirred for another 30 min. The resulting gel, with the molar composition 0.38 SiO_2:1 Al_2O_3:0.95 P_2O_5:1.14 DMAN:38 H_2O, was transferred to an autoclave with a Teflon liner and heated at 150 °C for 5 d under static conditions. Crystalline products were filtered and washed with abundant water and dried at 100 °C overnight. The samples were calcined at 550 °C in air to properly remove the precluded organic species.

Characterization. PXRD data were collected using a PANalytical X'Pert PRO Diffractometer with Bragg–Brentano geometry, using CuKα radiation (λ_1 = 1.5406 Å, λ_2 = 1.5441 Å, I_2/I_1 = 0.5; divergence slit: fixed = 1/16°; goniometer arm length: 240 mm; detector: PANalytical X'Celerator; tube voltage and intensity: 45 kV and 40 mA; scan range: 3.0° to 75.0° (2θ), scan step size: 0.017° (2θ); counting time: 2,400 s per step).

The chemical analyses were carried out on a Varian 715-ES ICP-Optical Emission spectrometer, after solid dissolution in HNO_3/HCl/HF aqueous solution. The organic content of as-made materials was determined by elemental analysis performed on an SCHN Fisons element analyzer. Thermogravimetric analysis was performed using a Mettler Toledo thermo-balance.

Textural properties were determined by Ar and N_2 adsorption–desorption isotherms measured at 87 K and 77 K, respectively, on a Micromeritics ASAP 2020.

The morphology of the samples was studied by SEM using a JEOL JSM-6300 microscope.

The solid-state NMR spectra were recorded at room temperature on a Bruker AV-400 spectrometer MAS. The ^{29}Si MAS NMR spectrum was performed with a spinning rate of 5 kHz at 79.459 MHz with a π/3 pulse length of 3.5 μs and repetition time of 180 s. The ^{27}Al MAS NMR spectrum was measured at 104.2 MHz with a spinning rate of 10 kHz and a π/12 pulse length of 0.5 μs with a 1-s repetition time. The solid-state ^{31}P MAS NMR spectrum was recorded at 161.9 MHz with a spinning rate of 10 kHz and a π/2 pulse of 5 μs with 20-s repetition time. The ^{13}C MAS NMR cross-polarization spectrum was achieved with a spinning rate of 5 kHz. ^{29}Si, ^{27}Al, ^{31}P, and ^{13}C chemical shifts were referenced to tetramethylsilane, $Al^{3+}(H_2O)_6$, 85% H_3PO_4, and adamantane, respectively. The ^{27}Al (triple-quantum) MAS NMR experiment was performed using z-filter pulse sequence.

Structure Elucidation. The calcined ITQ-51 sample was dispersed in absolute ethanol and treated by ultrasonification for 2 min. A droplet of the suspension was transferred onto a copper grid. The TEM sample was observed.

RED (39) was carried out on a JEOL JEM-2100 microscope operated at 200 kV using a single-tilt tomography sample holder. The 3D RED data collection was controlled by the RED data collection software package automatically (39). The selected-area electron diffraction (SAED) pattern was collected at each tilt angle from a submicrometer-sized crystal of ITQ-51. A typical tilt range was −60° to −70°, and the tilt step was 0.1° (*SI Appendix*, Table S1). The exposure time was 1 s per SAED pattern, and >1,300 SAED patterns could be collected in <2 h. The data processing of the >1,300 SAED patterns was performed using the RED data processing software package (39), which includes peak search, unit cell determination, indexation of reflections, and intensity extraction. The structure of ITQ-51 was solved by direct methods using the program SHELX based on the RED intensities. A complete structure determination of ITQ-51 from the RED data including data collection and processing, unit cell and space group determination, and structure solution and refinement could be done within 1 d, which is comparable to the time needed for structure determination by single-crystal X-ray diffraction. All framework atoms could be located and refined against the RED data.

The final structure model obtained from the RED data was refined by Rietveld refinement using TOPAS (48) with soft restraints for the T–O bond distances.

ACKNOWLEDGMENTS. The authors gratefully acknowledge Dr. Alejandro Vidal-Moya for the ^{27}Al MQ MAS NMR experiment. The authors also acknowledge financial support from Ministerio de Economía y Competitividad of Spain (MAT2012-37160), Consolider Ingenio 2010-MULTICAT, Generalitat Valenciana through the PROMETEO program, Universitat Politècnica de València through PAID-06-11 (n.1952), the Swedish Research Council (VR), the Swedish Governmental Agency for Innovation Systems (VINNOVA), and the Göran Gustafsson Foundation. M.M. also acknowledges "Subprograma Ramon y Cajal" for Contract RYC-2011-08972. The TEM used in this study was purchased from a grant by the Knut and Alice Wallenberg Foundation.

1. Corma A, Davis ME (2004) Issues in the synthesis of crystalline molecular sieves: Towards the crystallization of low framework-density structures. *ChemPhysChem* 5(3): 305–313.
2. Jiang J, Yu J, Corma A (2010) Extra-large-pore zeolites: Bridging the gap between micro and mesoporous structures. *Angew Chem Int Ed Engl* 49(18):3120–3145.
3. Cheetham AK, et al. (2001) Very open microporous materials: From concept to reality. *Stud Surf Sci Catal* 135, [CD-ROM] Paper 05-O-05 (Elsevier, 2001).
4. Annen MJ, Davis ME, Higgins JB, Schlenker JL (1991) VPI-7: The first zincosilicate molecular sieve containing three-membered T-atom rings. *J Chem Soc Chem Commun* (17):1175–1176.
5. Corma A, Díaz-Cabañas MJ, Jordá JL, Martínez C, Moliner M (2006) High-throughput synthesis and catalytic properties of a molecular sieve with 18- and 10-member rings. *Nature* 443(7113):842–845.
6. Jiang J, et al. (2011) Synthesis and structure determination of the hierarchical meso-microporous zeolite ITQ-43. *Science* 333(6046):1131–1134.
7. Wilson ST, Lok BM, Messina CA, Cannan TR, Flanigen EM (1982) Aluminophosphate molecular sieves: A new class of microporous crystalline inorganic solids. *J Am Chem Soc* 104(4):1146–1147.
8. Wilson ST, Flanigen EM (1986) Crystalline metal aluminophosphates. US Patent 4,567,029.
9. Pastore HO, Coluccia S, Marchese L (2005) Porous aluminophosphates: From molecular sieves to designed acids catalysts. *Annu Rev Mater Res* 35:351–395.
10. Bellussi G, Pollesel P (2005) Industrial applications of zeolite catalysts: Production and uses of light olefins. *Stud Surf Sci Catal* 158(B):1201–1213.
11. Hartmann M, Kevan L (2002) Substitution of transition metal ions into aluminophosphates and silicoaluminophosphates: Characterization and relation to catalysis. *Res Chem Intermed* 28(7–9):625–695.
12. Davis ME, Saldarriaga C, Montes C, Garces J, Crowder C (1988) A molecular sieve with eighteen-membered rings. *Nature* 331(6158):698–699.
13. Dessau RM, Schlenker JL, Higgins JB (1990) Framework topology of AlPO4-8: The first 14-ring molecular sieve. *Zeolites* 10(6):522–524.
14. Estermann M, McCusker LB, Baerlocher CH, Merrouche A, Kessler H (1991) A synthetic gallophosphate molecular sieve with a 20-tetrahedral-atom pore opening. *Nature* 352(6333):320–323.
15. Huo Q, et al. (1992) Synthesis and characterization of a novel extra large ring of aluminophosphate JDF-20. *J Chem Soc Chem Commun* (12):875–876.
16. Yang GY, Sevov SC (1999) Zinc phosphate with gigantic pores of 24 tetrahedra. *J Am Chem Soc* 121(36):8389–8390.
17. Lin CH, Wang SL, Lii KH (2001) [Ga2(DETA)(PO4)2]-2H2O (DETA = diethylenetriamine): A novel porous gallium phosphate containing 24-ring channels. *J Am Chem Soc* 123(19):4649–4650.
18. Davis ME (2002) Ordered porous materials for emerging applications. *Nature* 417(6891):813–821.
19. Curtis RA, Deem MW (2003) A statistical mechanics study of ring size, ring shape, and the relation to pores found in zeolites. *J Phys Chem B* 107(33):8612–8620.
20. Loiseau T, Ferey G (1994) Oxyfluorinated microporous compounds: VII. Synthesis and crystal structure of ULM-5, a new fluorinated gallophosphate $Ga_{16}(PO_4)_{14}(HPO_4)_2(OH)_2F_7$, $[H_3N(CH_2)_6NH_3]_4$, 6 H_2O with 16-membered rings and both bonding and encapsulated F^1. *J Solid State Chem* 111(2):403–415.
21. Sassoye C, Marrot J, Loiseau T, Ferey G (2002) Utilization of cyclopentylamine as structure directing agent for the formation of fluorinated gallium phosphates exhibiting extra-large-pore open frameworks with 16-ring (ULM-16) and 18-ring channels (MIL-46). *Chem Mater* 14(3):1340–1347.
22. Corma A, et al. (2010) Extra-large pore zeolite (ITQ-40) with the lowest framework density containing double four- and double three-rings. *Proc Natl Acad Sci USA* 107(32):13997–14002.
23. Freyhardt CC, Tsapatsis M, Lobo RF, Balkus KJ, Davis ME (1996) A high-silica zeolite with a 14-tetrahedral-atom pore opening. *Nature* 381(6580):295–298.
24. Wagner P, et al. (1997) CIT-5: A high-silica zeolite with 14-ring pores. *Chem Commun (Camb)* (22):2179–2180.
25. Burton AW, et al. (2003) SSZ-53 and SSZ-59: Two novel extra-large pore zeolites. *Chemistry* 9(23):5737–5748.
26. Lobo RF, Zones SI, Davis ME (1995) Structure-direction in zeolite synthesis. *J Inclus Phen Mol Rec* 21(1–4):47–78.
27. Staab HA, Saupe T (1988) "Proton sponges" and the geometry of hydrogen bonds: Aromatic nitrogen bases with exceptional basicities. *Angew Chem Int Ed Engl* 27(7): 865–879.

28. Llamas-Saiz AL, Faces-Foces C, Elguero J (1994) Proton sponges. *J Mol Struct* 328: 297–323.
29. Rodriguez I, Sastre G, Corma A, Iborra S (1999) Catalytic activity of proton sponge: Application to Knoevenagel condensation reactions. *J Catal* 183(1):14–23.
30. Corma A, Iborra S, Rodriguez I, Sanchez F (2002) Immobilized proton sponge on inorganic carriers: The synergic effect of the support on catalytic activity. *J Catal* 211(1): 208–215.
31. Gianotti E, Diaz U, Coluccia S, Corma A (2011) Hybrid organic-inorganic catalytic mesoporous materials with proton sponges as building blocks. *Phys Chem Chem Phys* 13(24):11702–11709.
32. Davis ME, Lobo RF (1992) Zeolite and molecular sieve synthesis. *Chem Mater* 4(4): 756–768.
33. Baerlocher CH, et al. (2007) Structure of the polycrystalline zeolite catalyst IM-5 solved by enhanced charge flipping. *Science* 315(5815):1113–1116.
34. Sun J, et al. (2009) The ITQ-37 mesoporous chiral zeolite. *Nature* 458(7242): 1154–1157.
35. Moliner M, et al. (2012) Synthesis design and structure of a multipore zeolite with interconnected 12- and 10-MR channels. *J Am Chem Soc* 134(14):6473–6478.
36. Willhammar T, et al. (2012) Structure and catalytic properties of the most complex intergrown zeolite ITQ-39 determined by electron crystallography. *Nat Chem* 4(3): 188–194.
37. Antonijevic S, et al. (2006) Dynamics on the microsecond timescale in microporous aluminophosphate AlPO-14 as evidenced by 27Al MQMAS and STMAS NMR spectroscopy. *J Am Chem Soc* 128(24):8054–8062.
38. Liu P, Ren J, Sun Y (2008) Influence of template on Si distribution of SAPO-11 and their performance for n-paraffin isomerization. *Microporous Mesoporous Mater* 114(1–3):365–372.
39. Zhang D, Oleynikov P, Hovmöller S, Zou XD (2010) Collecting 3D electron diffraction data by the rotation method. *Z Kristallogr* 225(2–3):94–102.
40. Wan W, Sun JL, Hovmöller S, Zou XD The Rotation Electron Diffraction (RED) software package—data collection and data processing. Available at www.calidris-em.com.
41. Strohmaier KG, Vaughan DEW (2003) Structure of the first silicate molecular sieve with 18-ring pore openings, ECR-34. *J Am Chem Soc* 125(51):16035–16039.
42. Pophale R, Cheeseman PA, Deem MW (2011) A database of new zeolite-like materials. *Phys Chem Chem Phys* 13(27):12407–12412.
43. Foster MD, Treacy MMJ (2010) A database of hypothetical zeolite structures. Available at www.hypotheticalzeolites.net/DATABASE/DEEM/, reference number 8236886.
44. Foster MD, Treacy MMJ Atlas of prospective zeolite structures. Available at www.hypotheticalzeolites.net/NEWDATABASE/index.html.
45. Baerlocher CH, McCusker LB Database of zeolite structures. Available at www.iza-structure.org/databases/.
46. Bennett JM, Kirchner RM (1992) The structure of calcined AlPO4-31—a new framework topology containing one-dimensional 12-ring pores. *Zeolites* 12(4):338–342.
47. O'Keeffe M, Peskov MA, Ramsden SJ, Yaghi OM (2008) The Reticular Chemistry Structure Resource (RCSR) database of, and symbols for, crystal nets. *Acc Chem Res* 41(12):1782–1789.
48. Young RA (1993) *The Rietveld Method. IUCr Book Serials* (Oxford Univ Press, New York).